RSC Advances

PAPER

View Article Online
View Journal | View Issue

Cite this: *RSC Adv.*, 2018, **8**, 29129

Comparative study of modified/non-modified aluminum and silica aerogels for anionic dye adsorption performance

Wentong Zhao,[a] Jing Zhu,[a] Wei Wei, *[ab] Lirong Ma,[a] Jianjun Zhu[a] and Jimin Xie *[a]

Received 28th June 2018
Accepted 29th July 2018

DOI: 10.1039/c8ra05532g

rsc.li/rsc-advances

Developing effective and low-cost adsorbents is of great significance for controlling water contamination. To eliminate anionic water contaminants, four modified/non-modified aluminum (Al_{HMD}, Al_{OSSD}) and silica (Si_{HMD}, Si_{OSSD}) aerogels have been successfully employed. The four as-prepared aerogels were applied as adsorbents for removal of an anionic dye (acid orange 7, AO) from aqueous solution. Compared to silica aerogels, aluminum aerogels showed efficient adsorption performance for anionic water contaminants. The AO maximum adsorption capacity of Al_2O_3 aerogel is twice as high as that of SiO_2 aerogel. The maximum adsorption capacity of aerogels was in the following order: Al_{HMD} > Al_{OSSD} > Si_{HMD} > Si_{OSSD}. Adsorption kinetics and isotherms of AO dye on the four as-prepared aerogels have also been studied. The kinetic data fitted well with the pseudo first-order kinetics model and the adsorption isotherm could be described by the Langmuir model. Adsorption rate of AO dye was mainly governed by film diffusion and intra-particle diffusion. Based on the adsorption mechanism, this work provides an idea for the design of superior adsorbents for anionic water contaminants.

Introduction

Water contamination is a very significant problem for human society due to tens of thousands of dyes being ubiquitous in sewage waters from multiple industries such as textiles, rubbers, cosmetics, food, printing, paper, carpets, leather, *etc.* Various methods for treatment have been developed, such as oxidation–ozonation,[1] photocatalysis,[2] coagulation–flocculation,[3] membrane separation,[4] biological methods[5] and adsorption.[6–8] Among these methods, the physical adsorption method is generally considered attractive owing to its effectiveness, ease of operation, convenience, simplicity of design, economic and environmental considerations, with the selection of adsorbent being the key to dye decolorization.[9]

Aerogels as a new type of nanometric materials, with low density, high porosity, and large specific surface area, are becoming the ideal choice of adsorbent.[10,11] To date, silica aerogels have been used for removal of dyes from aqueous solution as can be found in previous literature. Silica aerogels as sorbent materials were used to remove cationic dye rhodamine B from aqueous solutions by Li *et al.*[12] Hydrophobic/hydrophilic silica aerogel was successfully prepared to remove cationic dyes methylene blue and rhodamine B from aqueous solutions by Han *et al.*[13] Hydrophilic/hydrophobic transparent silica aerogel was synthesized to remove cationic dye rhodamine B from aqueous solutions by Zong *et al.*[14] Moreover, some other materials used for adsorption have also been reported. A nitrilotriacetic acid anhydride-modified lignocellulosic material was prepared to remove cadmium and lead from aqueous solutions by Huang *et al.*[15] The biosorption potential of dried activated sludge as a biosorbent for zinc(II) removal from aqueous solution was investigated by Yang *et al.*[16] A dried biomass waste from biotrickling filters has been prepared for removing lead [Pb(II)] ions from aqueous solutions by Cheng *et al.*[17] Summarizing the above literature, it was found that the composites as adsorbents were mostly studied for cationic dyes while the adsorption of anionic dyes has been treated much less. Water pollutants include not only cationic pollutants, but also anionic pollutants, so it is of great significance to study the adsorption of anionic pollutants.

The surface properties including surface areas and surface functional groups of aerogels can affect their adsorption capacity, and a larger specific surface area is beneficial to enhance adsorption capacity of adsorbents.[18,19] In this work, we combined the advantages of aluminum and silicon aerogels with a large surface area, and successfully prepared hexamethyldisilazane (HMDS)-modified Al_2O_3 aerogel (Al_{HMD}) and SiO_2 aerogel (Si_{HMD}) by an organic solvent exchange method. Adsorption capacities of the aerogels with different properties for the anionic dye acid orange 7 (AO) have been compared. The adsorption kinetic and isothermal parameters were evaluated. Experimental results suggested that the modified Al_2O_3 aerogel was more efficient, and Al_2O_3 aerogels were more suitable for

[a]*School of Chemistry and Chemical Engineering, Jiangsu University, Zhenjiang 212013, P. R. China. E-mail: weiwei@ujs.edu.cn&; xiejm391@sohu.com; Fax: +86 11 88791800; Tel: +86 11 88791708*

[b]*Center of Analysis and Test, Jiangsu University, Zhenjiang, 212013, P. R. China*

the removal anionic dye AO from aqueous solutions than SiO_2 aerogels.

Experimental

Materials

Aluminum isopropoxide (AIP) was chemically pure and obtained from Sinopharm Co. Ethanol (EtOH), HMDS ($C_6H_{19}NSi_2$), *n*-hexane (C_6H_{14}), ethyl silicate (TEOS), acetonitrile (C_2H_3N), nitric acid (HNO_3), ammonium hydroxide ($NH_3 \cdot H_2O$) and AO ($C_{16}H_{11}N_2NaO_4S \cdot 5H_2O$) were of analytical grade and obtained from Sinopharm Co. All chemicals were used without any further purification. The molecular structure of the AO is shown in Fig. 1. Deionized water was used throughout this work.

Aerogel synthesis

Synthesis of Al_2O_3 aerogel. Al_2O_3 wet gel was formed by the method of reflux in a water bath. AIP (2.5 g) was added to a round-bottom flask, after which the solution was heated to 80 °C with vigorous stirring. The volume ratio of deionized water to ethanol was 1 : 3. The solution was heated to reflux for 3 hours. Then the reaction mixture was heated at 80 °C for another 1 hour without stirring. A certain concentration of HNO_3 was added to the solution, after which the solution was moved to a beaker and cooled to room temperature. The sol was stirred for 1 hour and aged for several days. The Al_2O_3 wet gel was thus prepared. The drying method adopted was one of two ways. The first way was hydrophobic modification drying (HMDS). Briefly, the gel was aged in EtOH and soaked in C_6H_{14}, $C_6H_{19}NSi_2/C_6H_{14}$ (at a volume ratio of 1 : 2) and C_6H_{14} in turn. Then the aerogel was formed after drying at 60 °C for 12 hours in an oven. The obtained Al_2O_3 aerogel was named Al_{HMD}. The other way was organic solvent sublimation drying (OSSD). The wet gel was aged in EtOH and soaked in 50%, 80%, 100% exchanging solvent C_2H_3N/EtOH (v/v) for every 12 h, and then dried at 50 °C under 80–100 kPa in a vacuum drying oven. The obtained Al_2O_3 aerogel was designated Al_{OSSD}. The chemical principle for the preparation of the Al_2O_3 aerogels is depicted in Fig. 2.

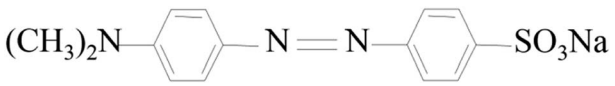

Fig. 1 Chemical structure of dye acid orange 7.

Synthesis of SiO_2 aerogel. SiO_2 wet gel was obtained by the method of acid and base two-step catalysis.[13] The sol was prepared with the following reagent volume proportion: TEOS5.5 : EtOH5.75 : $HNO_3$1.8 (0.008 M). Then the sol was formed after stirring for 12 hours. An amount of 0.15 mL (0.5 M) of $NH_3 \cdot H_2O$ was added to the sol and stirred for several minutes, affording the SiO_2 wet gel after standing. The wet gel was dried using the two drying methods mentioned above. The obtained SiO_2 aerogels were denoted Si_{HMD} and Si_{OSSD}, respectively.

Characterization

The small angle X-ray diffraction (SAXD) patterns of samples were obtained with a D/Max-γA X-ray diffractometer (Rigaku, Tokyo, Japan) at 40 kV and 100 mA with monochromatic Cu (divergence slit (DS) = 0.1°, scattering slit (SS) = 0.1°, receiving slit (RS) = 0.15 mm, scan 0.6–10°, rate of scanning 0.5° min^{-1}). The microstructures of the aerogels were observed with

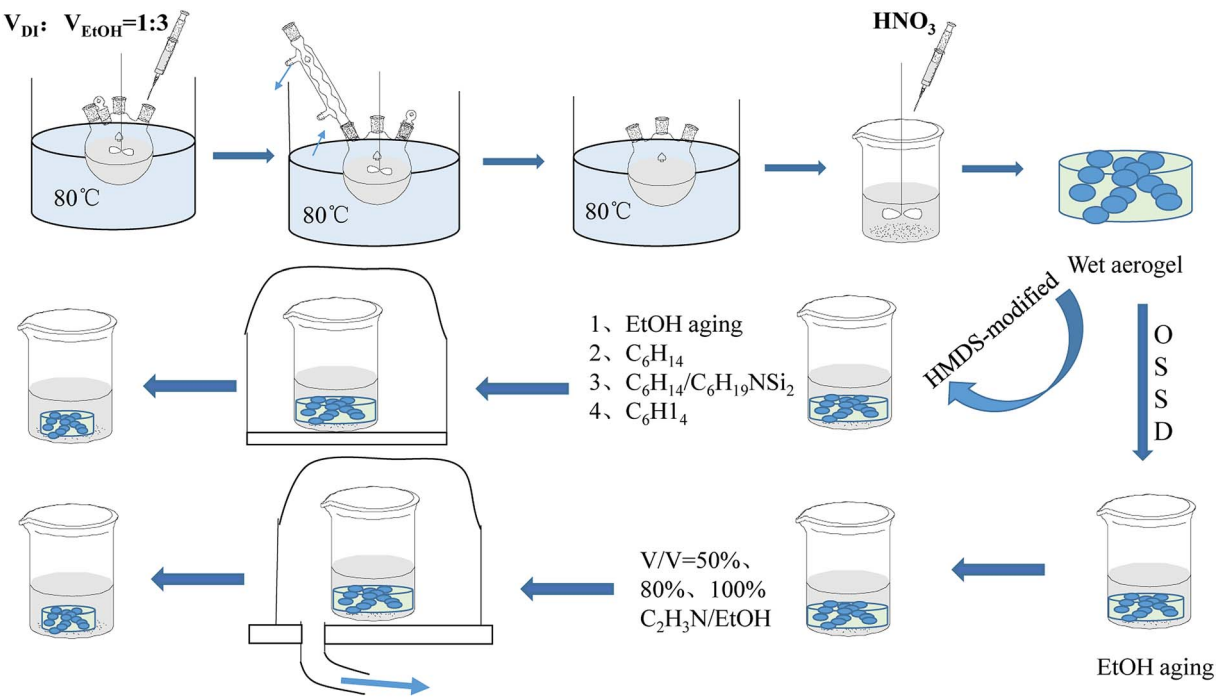

Fig. 2 The chemical principle for preparation of Al_2O_3 aerogels.

scanning electron microscopy (SEM, Philips XL-30SEMAnalyzer) and transmission electron microscopy (TEM, Philips Tecnnai-12, operating at 120 kV). Contact angles were measured by using a contact angle system (Harke-SPCA, Harke, China). The Brunauer–Emmett–Teller (BET) specific surface area was obtained from N_2 adsorption/desorption analyses at 77 K (NOVA2000; Quantachrome, Boynton Beach, FL). Pore size distribution and pore volume were calculated by the Barrett–Joyner–Halenda method. Mutual effects between the modifier and the wet gel were analyzed by Fourier transform infrared (FT-IR) spectra, which were obtained with the KBr wafer technique. The spectra were recorded from 500 to 4000 cm^{-1}. The concentration of dyes was determined using a UV-visible spectrophotometer (UV-2450; Shimadzu, Kyoto, Japan).

Adsorption experiment of AO

An accurately weighed quantity of the dye AO was dissolved in deionized water to prepare stock solution (500 mg L^{-1}). To prevent decolorization by direct sunlight, the stock solutions were stored in a dark bottle and kept in a dark place before use. Experimental solutions of the desired concentration were obtained by successive dilutions the stock solution in definite proportions.

All adsorption experiments were conducted by batch experiments mixing 0.02 g aerogel powder with 20 mL AO aqueous solution of known concentration in a series of 50 mL conical flasks. The mixture in a flask with the required concentration and appropriate pH was shaken at a speed of 180 rpm in a constant temperature oscillator at room temperature.[20] The dye solution pH was adjusted to different values between 1 and 13 with hydrochloric acid (0.1 M) or sodium hydroxide solution (0.1 M). After a fixed time interval, the suspension was centrifuged. The residual concentrations of the solutions were measured by a UV-visible spectrophotometer.

The equilibrium adsorption capacity Q_e (mg g^{-1}) and percentage removal of aerogel powder for AO aqueous solution were calculated through the following equations:

$$Q_e = \frac{(C_0 - C_e)V}{m} \quad (1)$$

$$\text{Percentage removal} = \frac{100(C_0 - C_e)}{C_0} \quad (2)$$

where C_0 (mg L^{-1}) and C_e (mg L^{-1}) are the initial and equilibrium adsorbate concentrations of AO in the solution, respectively; V (L) and m (g) are the volume of solution and the mass of adsorbent, respectively.

The data of equilibrium obtained were analyzed using Langmuir and Freundlich isotherm models, which can be described as:

$$\frac{1}{Q_e} = \frac{1}{Q_m} + \left(\frac{1}{bQ_m}\right)\left(\frac{1}{C_e}\right) \quad (3)$$

$$\log Q_e = \log K_f + \frac{1}{n} \log C_e \quad (4)$$

where Q_m (mg g^{-1}) and b (L mg^{-1}) are the maximum adsorption capacity and Langmuir constant related to the energy of adsorption, respectively. K_f (mg g^{-1}) is the Freundlich constant related to the adsorption capacity and n is an empirical constant.

The linearized pseudo-first-order Lagergren equation is expressed as:

$$\log(Q_e - Q_m) = \log Q_e - k_1 t/2.303 \quad (5)$$

where k_1 (min^{-1}) and t (min) are the adsorption equilibrium rate constant of pseudo-first-order kinetics and contact time, respectively.

Results and discussion

Physicochemical properties of the as-prepared aerogels

The SAXD patterns of the as-prepared aerogels are shown in Fig. 3(a). It can be seen that the samples of Al_{HMD}, Al_{OSSD} and Si_{HMD} showed diffraction peaks in the position of 1° to 2°, and all the diffraction peak positions were at approximately 1°. This indicates that the three aerogels possess similar mesoporous structure and aperture. The diffraction peak of Si_{OSSD} is indistinct in comparison with the others. This indicates that the regularity of mesopores in Si_{OSSD} was poorer than in the others.[21] Thus it can be seen that HMDS modification made the internal structure change in the silica aerogel.

For further research on the influence of the drying method on aerogel structure, the FT-IR spectra were studied. Fig. 3(b) shows the FT-IR spectra of the as-prepared aerogels. As can be seen from the figure, after using the HMDS modification drying, the hydroxyl peak of Al_{HMD} and Si_{HMD} became weaker than that of Al_{OSSD} and Si_{OSSD} at 3480 cm^{-1}. This is because the –OH group on the aerogel surface was replaced by the organic group after modification drying. The medium width adsorption band near 1634 cm^{-1} in the spectrum of Al_{OSSD} can be attributed to the bending vibration of H_2O.[22] The absorption peaks of Al_{HMD} and Al_{OSSD} near 1063 cm^{-1} can be ascribed to Al–O–Al vibrations, and absorption bands near 753 cm^{-1} can be attributed to bending of the O–Al–O bonds. The peaks at 2987 cm^{-1}, 1360 cm^{-1} and 926 cm^{-1} correspond to the asymmetric, symmetric and in-plane vibrations of $-CH_3$ group. This indicates whether the modification of Al_2O_3 aerogel has no influence on the existence of methyl. As seen from Fig. 3(b), the Si_{HMD} shows asymmetric methyl vibration and swing vibration at 2958 cm^{-1} and 901 cm^{-1}, respectively, compared with Si_{OSSD}. It can be inferred that the silica aerogel contains methyl on the surface after modification drying.[23] The absorption peaks of Si_{HMD} and Si_{OSSD} near 1061 cm^{-1} can be ascribed to Si–O–Si vibrations, and absorption bands near 789 cm^{-1} can be attributed to bending of the O–Si–O bonds.

Fig. 4 presents SEM micrographs of the four as-prepared aerogels. Fig. 4(a) displays the SEM image of Al_{HMD}, the structure of which presents porous agglomerates composed of Al_2O_3 particles.[24] Compared with the compact stacked bulk morphology of Al_{OSSD}, Al_{HMD} has a more fluffy and porous sheet structure. As can be seen from the SEM image (Fig. 4(c)) of

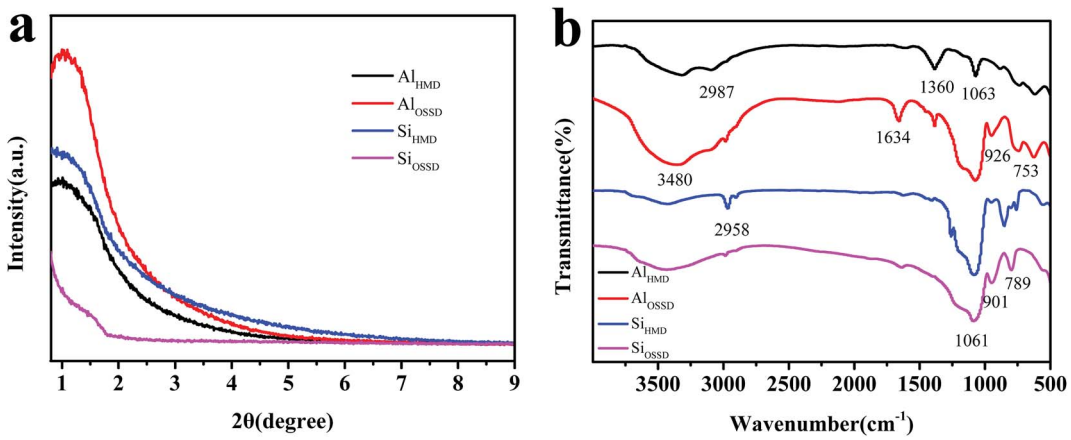

Fig. 3 SAXD patterns (a) and FT-IR spectra (b) of the as-prepared aerogels.

Si_{HMD}, it exhibits 20–50 nm colloidal particles constituting a three-dimensional branching network structure,[25] but Si_{OSSD} tends to be agglomerated into bulk in Fig. 4(d). In short, Al_{OSSD} and Si_{OSSD} aerogels dried through OSSD consist of agglomeration of several micrometers or hundreds of micrometers. The agglomeration dimension of Al_{OSSD} is smaller than that of Si_{OSSD}. On the basis of this, it is speculated that the size of agglomeration is the reason why the adsorption capacity of Al_2O_3 aerogel better than that of SiO_2 aerogel.[26]

The TEM images of the as-prepared aerogels are shown in Fig. 5. As shown in Fig. 5, the compositions of the aluminum-based aerogels are dense and pleated, and the compositions of the silica-based aerogels are more loose and porous. In order to determine the hydrophobic conditions of aerogels, the contact angle of sample and water was measured, as shown in the insets of Fig. 5. The contact angle of Al_2O_3 aerogel and water is much less than 90°, presenting ease of wetting by water and good hydrophilic energy (insets in Fig. 5(a and b)). The inset of Fig. 5(c) shows the water droplet on the surface of the HMDS-modified SiO_2 aerogel is basically spherical, the water contact angle being more than 90° and not easily wetted by water, exhibiting good hydrophobic properties. This shows that the modified aerogel surface organic groups have excellent hydrophobic properties.[27] The water contact angle of SiO_2 aerogel dried by OSSD is much less than 90°, showing good hydrophilic properties (inset in Fig. 5(d)). The water contact angle of aerogels dried by OSSD approaches 0°, indicating super-hydrophilic properties (insets in Fig. 5(b and d)).

The aerogel powder textural properties were further analyzed by BET adsorption–desorption measurements. The N_2

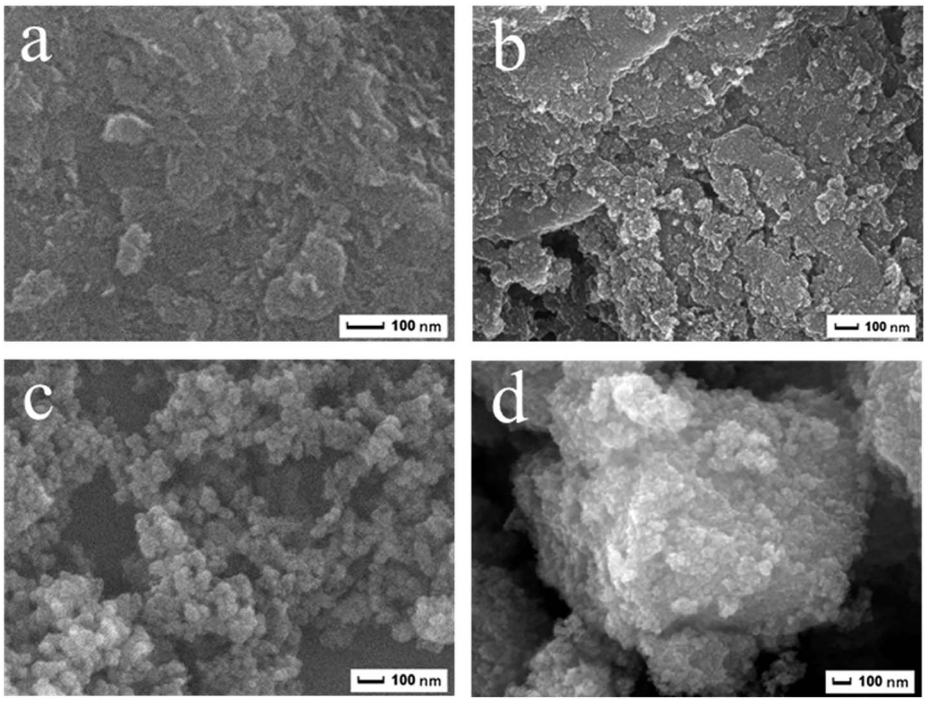

Fig. 4 SEM micrographs of the as-prepared aerogels: (a) Al_{HMD}, (b) Al_{OSSD}, (c) Si_{HMD} and (d) Si_{OSSD}.

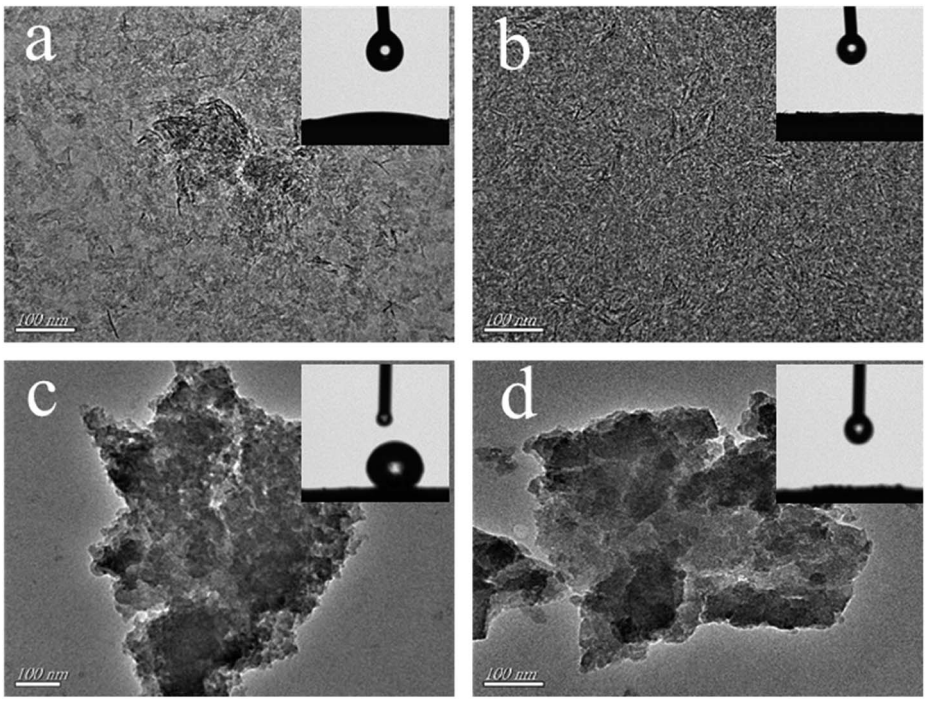

Fig. 5 TEM images and water contact angle (insets) of the as-prepared aerogels: (a) Al_{HMD}, (b) Al_{OSSD}, (c) Si_{HMD} and (d) Si_{OSSD}.

adsorption–desorption isotherms and pore size distribution curves of the as-prepared aerogels obtained at 77 K are shown in Fig. 6. The adsorption and desorption isotherms obtained for all samples are of type IV which is the performance characteristic of mesoporous materials according to the classification by IUPAC, as shown in Fig. 6(a and b).[28–30] The hysteresis loop in the isotherms is caused by the capillary condensation of N_2 gas occurring in the mesopores. The shape of the pores determines the hysteresis loop shape.[31] The Al_{HMD} sample shows H1 type of hysteresis loop, while the other samples present the shape of the hysteresis loop between type H_2 and H_3.[32,33]

In addition, the four as-prepared aerogel pore size distributions are depicted in Fig. 6(c–f). The pore size distributions are unimodal with the peak of Al_{HMD}, Al_{OSSD}, Si_{HMD} and Si_{OSSD} pore radius at 20, 10, 3 and 5 nm, respectively. The monomodal pore size distribution indicates the mesoporous nature of the

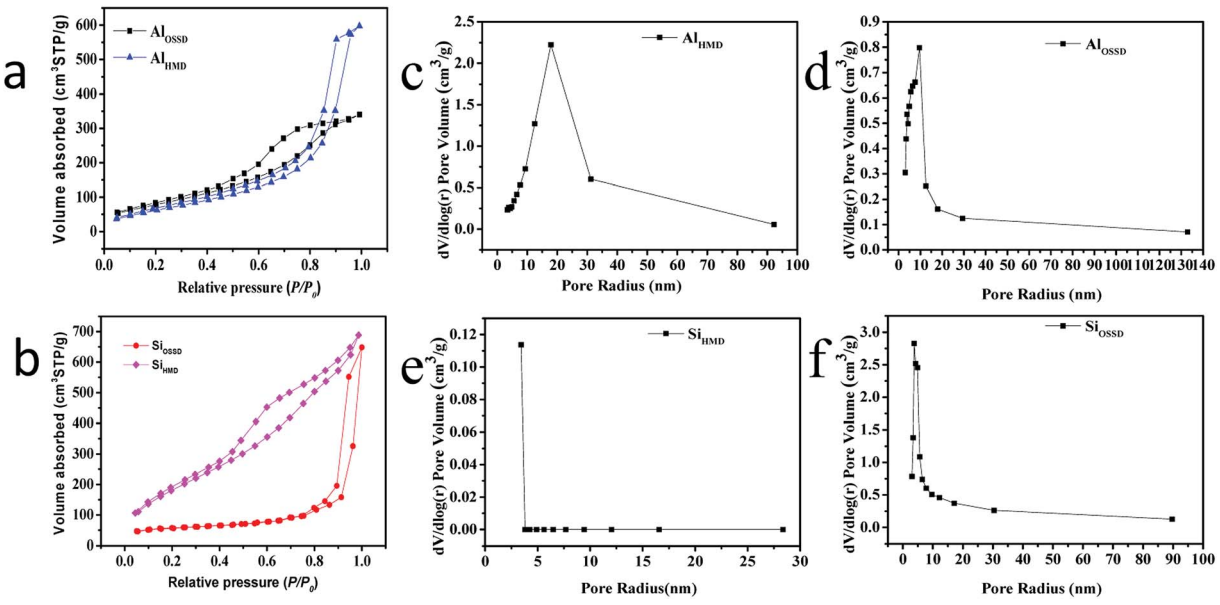

Fig. 6 (a and b) Adsorption–desorption nitrogen isotherms and (c–f) pore size distribution curves of the as-prepared aerogels: (a) modified/non-modified Al_2O_3 aerogels, (b) modified/non-modified SiO_2 aerogels, (c) Al_{HMD}, (d) Al_{OSSD}, (e) Si_{HMD} and (f) Si_{OSSD}.

synthesized aerogels. The BET surface area, pore volume, and average pore radius of the four as-prepared aerogel samples are summarized in Table 1. For alumina aerogels, the aerogel modified/non-modified by HMDS is not significantly different in terms of surface area. But the pore radius of Al_2O_3 aerogel after HMDS modification (17.865 nm) is about three times that prepared by OSSD (5.622 nm). This shows that the modification has little effect on the specific surface area of the aluminum aerogel but it does affect the pore size. On the contrary, the surface area of silica aerogel is significantly increased after the surface modification of HMDS (671.762 $m^2\ g^{-1}$) compared to the OSSD method (151.240 $m^2\ g^{-1}$) and the pore size distribution is almost the same. This indicates that the modification has a great influence on the specific surface area of the silica aerogel, but hardly affects the size of the pores.

The as-prepared aerogels are porous materials which are composed of colloidal agglomerations of different dimensions. The FT-IR analysis and water contact angle illustrate that modification reduces hydroxyl groups on the surface of aerogels and results in the hydrophobicity of Si_{HMD}. For the four as-prepared aerogels, the aluminum-based aerogels have moderate specific surface area and larger pore radius after modification. For the silica-based aerogels, the non-modified aerogel has a lower specific surface area while the modified aerogel has a larger specific surface area; but both of the aerogels have almost the same pore size. The data for specific surface area and porosity can benefit the contact between the adsorption sites of aerogels and AO molecules. To sum up, the as-prepared aerogels can be used as adsorbents because they are good porous materials and easily modified by functional groups.

Table 1 Textural parameters deduced from N_2 adsorption at −196 °C of the as-prepared aerogels

Sample	Surface area ($m^2\ g^{-1}$)	Pore volume ($cm^3\ g^{-1}$)	Pore radius (nm)
Al_{OSSD}	364.601	0.528	5.622
Al_{HMD}	330.096	0.944	17.865
Si_{OSSD}	151.240	0.281	3.419
Si_{HMD}	671.762	0.987	3.793

Factors affecting dye adsorption

In order to investigate the adsorption properties of the as-prepared aerogels for anionic dyes, the solution pH, contact time, and initial dye concentration will be taken into consideration. The influence of these various parameters on the removal of AO dye is studied as follows.

Effect of solution pH and zeta potential. The pH of the dye solution plays an important role in AO dye treatment process, particularly for the adsorption capacity.[34] The efficiency of adsorption depends on the solution pH because variation in pH brings about a variation in the surface properties of the adsorbent and the degree of ionization of the adsorbate molecules present in the solution.[35,36] Gupta *et al.*[37] studied the effect of solution pH on the adsorption of AO by waste materials (bottom ash and de-oiled soya) and they discovered that the maximum adsorption was at pH 2.

Fig. 7 shows the adsorption capacity of all of the prepared aerogels for AO at pH varying in the range of 1–13. The maximum removal rates of AO for the four prepared aerogels are at pH = 2, pH = 4, pH = 3 and pH = 3, respectively. From Fig. 7 and considering the optimization of subsequent experimental conditions, all subsequent experiments were implemented at pH 3. As shown in Fig. 7, when the pH is less than 7, the all aerogels adsorb AO and the removal rate increases first then decreases with the increase of pH. When the initial pH is more than 7, there is almost no adsorption capacity for anionic dye AO of the aerogels. This is because of the presence of excessive OH^-, which competes with the dye anions for the adsorption sites at alkaline pH.[38] In Fig. 7(a), the maximum AO removal rate of Al_{HMD} is 42.3%, which is about 5% higher than the maximum adsorption rate of Al_{OSSD} of 37.6%. The AO removal rates of Si_{HMD} and Si_{OSSD} only show a slight change in Fig. 7(b). The reason why the removal efficiency of silica aerogels before and after the modification is not significantly improved may be that the pore radius of the silica aerogel before and after the modification does not change significantly. The alumina aerogels have a larger pore radius than the silica

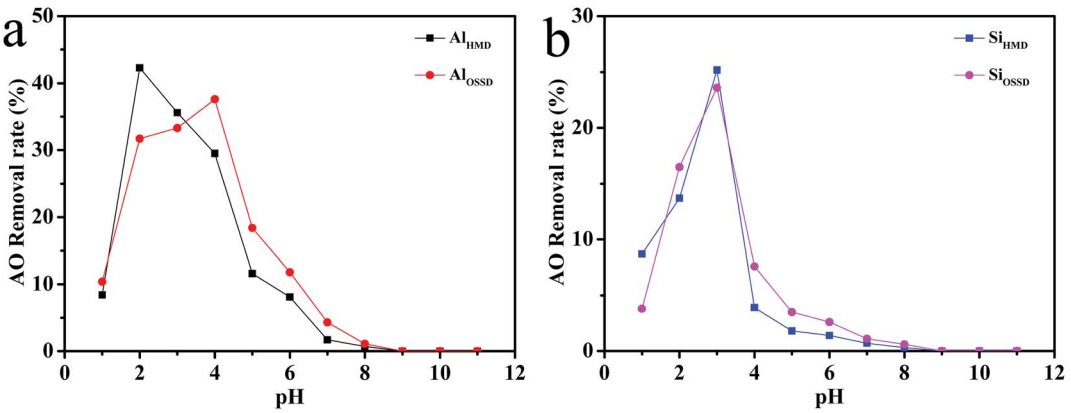

Fig. 7 Effect of initial solution pH on the adsorption of AO dye on the as-prepared aerogels: (a) Al_{HMD} and Al_{OSSD}, (b) Si_{HMD} and Si_{OSSD} (0.02 g adsorbent, 20 ml of 10 mg L^{-1} AO dye, oscillation time of 12 h).

aerogels, and the maximum removal rate of Al_2O_3 aerogel for AO is twice that of the SiO_2 aerogel at acidic pH. Therefore, this further confirmed that the pore radius of the aerogel is one of the important parameters affecting the AO removal rate.

The surface properties of adsorbents are also important factors in the dye adsorption process. Zeta potential is the potential difference between the dispersion medium and the stationary layer of fluid attached to a dispersed particle.[39] Thus, zeta potential is used to determine the potential of aerogel surface to confirm the results of adsorption. The surfaces of the four as-prepared aerogels (Al_{HMD}, Al_{OSSD}, Si_{HMD}, and Si_{OSSD}) have charges of +0.83 mV, −0.34 mV, −4.34 mV, and −4.43 mV, respectively. This indicates that the surfaces of the aerogels are negatively charged, except Al_{HMD}. The positively charged surfaces can enhance the adsorption of the negatively charged AO anions by the adsorbents through electrostatic forces of attraction.[40] One is able to infer the adsorption capacity of the four as-prepared aerogels is in the order Al_{HMD} > Al_{OSSD} > Si_{HMD} > Si_{OSSD} according to the size of the zeta potential. Meanwhile, it has been reported that for a certain range of electrolyte concentrations, for colloidal particles of the same size and surface charge density, the surface of the particles is different in hydrophilicity and the electrophoretic mobility is different.[41–43] Since the surface charge is surrounded by the hydrophilic layer, and the hydrophilic surface increases the bonding of the ions and increases the surface conductance and causes the shear plane to expand, the hydrophilic surface of aluminum aerogels causes a decrease in the electrophoretic mobility and absolute values of the zeta potential. Moreover, Leonard *et al.*[44] have reported that using materials that have different surface potentials causes an increased attraction of ions during the removal process. Suchithra *et al.*[45] have reported that the surface charge affects the adsorption process, negative surface charge attracting ions carrying net positive surface charge. So, it can be concluded that the surface charge of the materials is also an important factor of adsorption.

Effect of contact time. The contact time between adsorbent and adsorbate is also an important physical parameter in industrial wastewater treatment.[46] From Fig. 8 it is clear that rapid adsorption of AO dye took place within 30 min for the four prepared aerogels, and then adsorption became slow and almost reached equilibrium within 120 min. At the initial contact time the adsorption sites are exposed and these make the rate of adsorption to be fast, and, consequently, the diffusion process from the bulk solution to the adsorption sites.[47] It is also seen from Fig. 8 that the removal of dye by adsorption on aerogels is very fast at the initial period of contact but slowed down with time. This is because each adsorbent has limited adsorption sites and, after a certain time, these are exhausted and the adsorption process attained an equilibrium state.[48] More importantly, the Al_2O_3 aerogel exhibited twice the adsorption rate compared to the SiO_2 aerogel, which can be ascribed to the surface potential and active groups. As can be seen from Fig. 8, the adsorption capacity of the four as-prepared aerogels is in the order Al_{HMD} > Al_{OSSD} > Si_{HMD} > Si_{OSSD}.

Effect of initial AO dye concentration. The initial dye concentration has a pronounced effect on its removal from aqueous solutions.[49] The adsorption capacity for AO dye of the four as-prepared aerogels increases with the initial dye

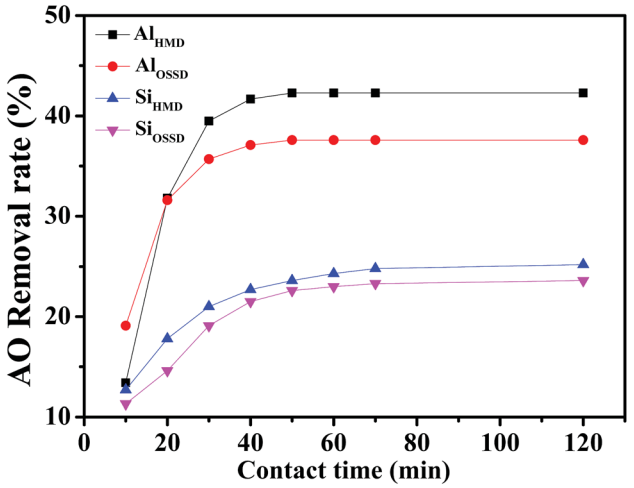

Fig. 8 Effect of contact time on the adsorption of AO dye on the as-prepared aerogels (0.02 g adsorbent, pH = 3, 20 ml of 10 mg L^{-1} AO dye): (a) Al_{HMD}, (b) Al_{OSSD}, (c) Si_{HMD} and (d) Si_{OSSD}.

concentration as shown in Fig. 9. It is found that when the initial dye concentration increases from 10 to 200 mg L^{-1}, the adsorption capacity of AO onto Al_2O_3 aerogel is 3.7 to 52 mg g^{-1} and the adsorption capacity of AO onto SiO_2 aerogel is 2.36 to 20.2 mg g^{-1}. Basically, from Fig. 9, the adsorption percentage decreases and the adsorption capacity increases with increasing initial dye concentration. It is likely that the resistance to mass transfer of dye between the aqueous solution and the solid phase is overcome by the driving force provided by the initial dye concentration. Perhaps the higher initial concentration solutions have stronger driving forces in adsorption and fewer available adsorption sites of constant adsorbent compared to the lower initial concentration solutions, so AO removal depends upon the initial concentration.[50] Besides, with the increase in initial concentration, the interaction between dye and adsorbent is enhanced. Therefore, the increase of the adsorption of dye will follow the increase in initial dye concentration.

Adsorption kinetics

The study of adsorption kinetics is a prerequisite for the quantitative description of the course of a reaction with time, giving valuable insights into the chemical reaction and mechanism of the adsorption process. The time *versus* $\log(Q_e - Q_m)$ plots (Lagergren plots) were found to be linear for the four as-prepared aerogels, as shown in Fig. 10. The calculated kinetic parameters from these plots such as rate constants and correlation coefficients R^2 for the different aerogels are given in Table 2. It is clear that high correlation coefficients (R^2 > 0.99) were observed for all fits, the AO adsorption process being of a pseudo-first-order nature in each case. The slope values evaluated from these straight line plots for Al_{HMD}, Al_{OSSD}, Si_{HMD}, and Si_{OSSD} are found to be -5.613×10^{-2}, -5.203×10^{-2}, -2.405×10^{-2}, and -2.800×10^{-2}, respectively. Results show that the overall AO adsorption process rate should be controlled by the chemical process in conformity with the pseudo-first-

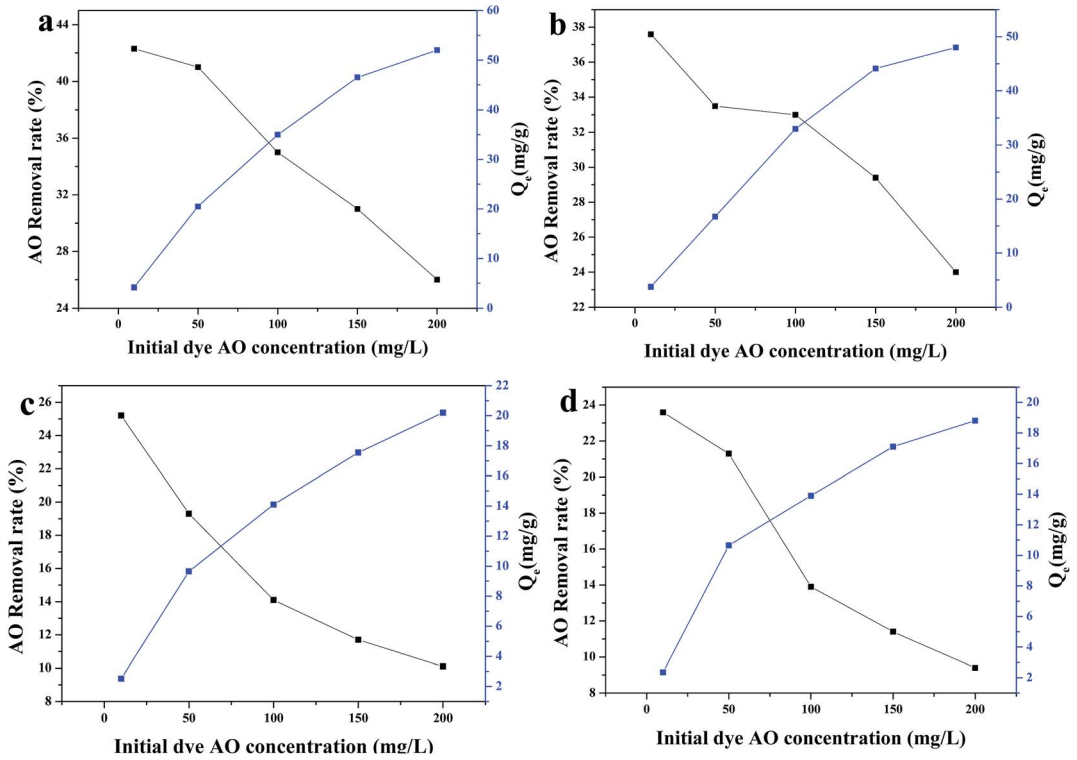

Fig. 9 Effect of initial AO dye concentration on the adsorption of AO on the as-prepared aerogels (0.02 g adsorbent, 20 ml of AO dye, initial dye concentration = 10–250 mg L^{-1}, pH = 3, contact time = 12 h): (a) Al_{HMD}, (b) Al_{OSSD}, (c) Si_{HMD} and (d) Si_{OSSD}.

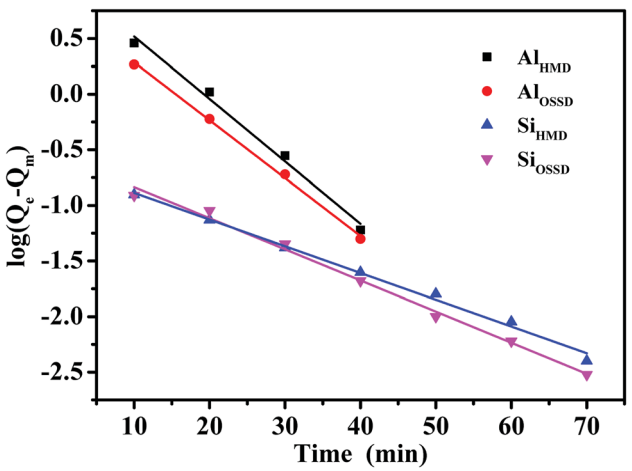

Fig. 10 Lagergren plot for the adsorption of AO dye on the four as-prepared aerogels.

Table 2 Rate constants obtained from Lagergren rate equation for adsorption of AO dye on the four as-prepared aerogels

Sample	Slope	Intercept	Rate constant, k_1 (min^{-1})	R^2
Al_{HMD}	-5.613×10^{-2}	1.080	0.013	0.9914
Al_{OSSD}	-5.613×10^{-2}	0.807	0.002	0.9987
Si_{HMD}	-2.405×10^{-2}	−0.646	0.010	0.9994
Si_{OSSD}	-2.800×10^{-2}	−0.555	0.015	0.9992

order kinetics mechanism. Adsorption kinetics reveals the rate of solute uptake and evidently this rate controls the residence time of the AO dye at the solution interface.

Mass transfer of an adsorbate to an adsorbent particle is governed by a number of relationships obtained mainly from diffusion and mass balance equations. There may occur three consecutive steps in the process of organic matter adsorbed to porous adsorbents from aqueous solution, and these steps are as follows: (i) film diffusion, where the adsorbate is instantaneously transferred to the adsorbent exterior through available

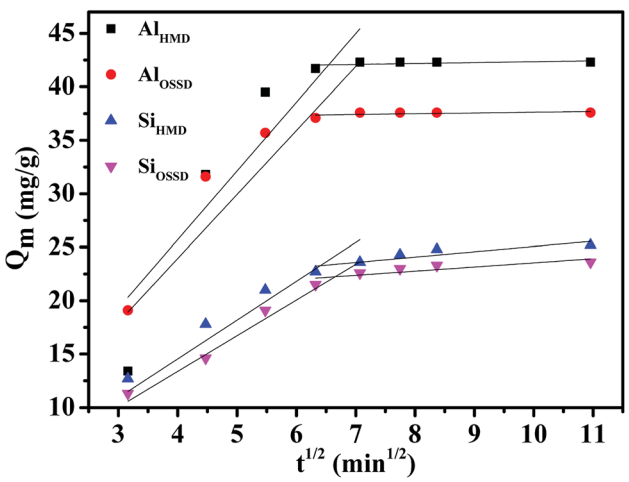

Fig. 11 Kinetic plots of intra-particle diffusion model for the adsorption of AO dye on the four as-prepared aerogels.

Table 3 Kinetic parameters obtained from intra-particle diffusion model for adsorption of AO dye on the four as-prepared aerogels

	First stage		Second stage	
Sample	k_i	R^2	k_i	R^2
Al_{HMD}	6.425	0.9827	0.085	0.9984
Al_{OSSD}	5.985	0.9874	0.071	0.9886
Si_{HMD}	3.635	0.9940	0.498	0.9981
Si_{OSSD}	3.343	0.9982	0.387	0.9991

active sites on the surface film; (ii) particle diffusion, where the adsorbate molecules migrate from the surface to the interior of the adsorbent particle; and (iii) equilibrium, where the adsorption of the adsorbate occurs on the inner surface of the adsorbent.[36]

The intra-particle diffusion model was used to identify the diffusion mechanism during the AO adsorption process.[51] It is described using the following equation:

$$Q_m = k_i t^{1/2} + C \quad (6)$$

where k_i (mg g^{-1} min$^{-1/2}$) is the intra-particle diffusion constant and C is a constant which describes the boundary layer effects.

Fig. 11 depicts that the intra-particle diffusion model for AO adsorption fitted well ($R^2 > 0.98$) the data if the whole adsorption process was divided into two linear phases involving a first stage and a second stage. The two phases in the intra-particle diffusion plot represent surface adsorption to the adsorbent and the intra-particle diffusion of AO to adsorption sites.[52] The intra-particle diffusion rate constant k_i (mg g^{-1} min$^{-1/2}$) is evaluated from the slope of the second linear portion of Q_m *versus* $t^{1/2}$, the values being presented in Table 3. Initially, within the first stage, it is postulated that AO molecules from bulk solution are transported to the external aerogel surface through film diffusion and its rate is very high. A larger slope can be observed from the first sharp section suggesting that the rate of dye removal is higher firstly attributed to the active adsorption sites. After saturation of the surface, the AO molecules enter into the aerogel by intra-particle diffusion until equilibrium is reached. Hence, the AO adsorption process might be described by film diffusion followed by intra-particle diffusion process.[53]

Adsorption isotherms

The adsorption isotherms show the adsorbed molecules are distributed at the interface between the solid phase and the liquid phase when the adsorption process reaches an equilibrium state. To analyze the adsorption equilibrium data by fitting them to different isotherm models is of fundamental importance to find the suitable model that can be applicable for design purposes.[54] There are several isotherms such as the Langmuir and Freundlich models, which are most widely

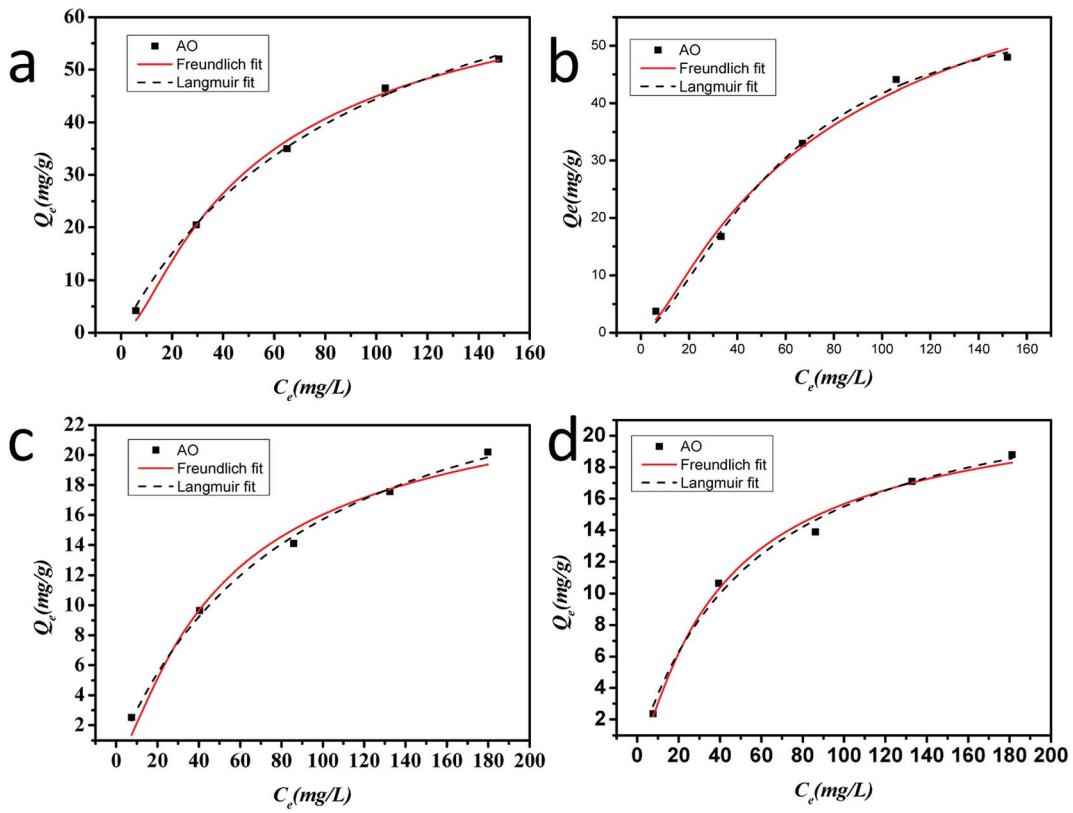

Fig. 12 Langmuir and Freundlich adsorption isotherms for the adsorption of AO dye on the four as-prepared aerogels: (a) Al_{HMD}, (b) Al_{OSSD}, (c) Si_{HMD} and (d) Si_{OSSD}.

used to describe the adsorption isotherms. The Freundlich and Langmuir adsorption isotherm models were each successfully applied to the adsorption capacity variation *vs.* concentration for the four as-prepared aerogels, shown in Fig. 12, and the parameters and correlation coefficients calculated for the Langmuir and Freundlich linear models are given in Table 4. Normally the best-fitting model can be chosen based on the linear regression correlation coefficient (R^2) values. Table 4 shows that the least-squares correlation coefficient (R^2) values of the Langmuir model are higher than those of the Freundlich model for all samples, which demonstrate that the isotherms of all of samples are well fitted by the Langmuir equation.

The kinetic data are well fitted with the Lagergren first-order kinetics model according to the adsorption kinetics and the isotherm adsorption data are well fitted with the Langmuir model. The results of kinetic experiments and Langmuir isotherm confirm that, for all adsorbents, the adsorption proceeds *via* film diffusion and intra-particle diffusion.

In consideration that dyes have high molecular weight and complex structures, the as-prepared aerogels are used for adsorption of small molecule ions to compare the results with the adsorption of dyes.

Adsorption mechanism

There are no chemical bonds produced between the aerogel and AO dye, and thus the adsorption process is physical adsorption. The adsorption capacity is compared with the theoretical model, and the adsorption capacity of the aluminum aerogel is superior to that of the silica aerogel, with the modified aerogel being better than the non-modified aerogel. This indicates that the modification could promote adsorption. The data of specific surface area and porosity can benefit the contact between the adsorption sites of aerogels and AO molecules. The aluminum aerogel has stronger adsorption capacity than the silica aerogel due to the positively charged surfaces of the aluminum aerogel being able to provide adsorption sites for electrostatic interaction with negatively charged AO dye molecules. The reason why Si_{HMD} has the largest specific surface area but lower adsorption capacity is the electrostatic repulsion between the negatively charged active sites on the adsorbent and the anionic AO dye molecules.

Table 4 Isotherm parameters and standard error (SE, %) in Langmuir and Freundlich equations for adsorption of AO dye on the four as-prepared aerogels

Sample		Al_{OSSD}	Al_{HMD}	Si_{OSSD}	Si_{HMD}
Langmuir isotherm	Q_m	60.07973	86.3646	24.51519	29.63243
	b	3.39956	0.99545	0.46829	0.19645
	R^2	0.99023	0.99739	0.98892	0.99596
	SE	8.62653	4.82465	1.6492	1.62894
Freundlich isotherm	$1/n$	5.90108	2.17416	0.47127	0.97353
	K_f	87.35538	76.325	23.62971	26.62134
	R^2	0.98304	0.99429	0.98885	0.97999
	SE	28.30551	3.40973	1.07399	1.91506

Conclusion

In summary, a comparative study of modified/non-modified aluminum and silica aerogels used to remove the dye AO is presented. HMDS-modified Al_{HMD} aerogel and Si_{HMD} aerogel show smaller colloidal agglomerates than Al_{OSSD} and Si_{OSSD}. The surface area of Al_{HMD} aerogel has a slight change (from 364.601 to 330.096 $m^2\ g^{-1}$) after being modified by HMDS; the surface area of Si_{HMD} aerogel increased from 151.240 to 671.762 $m^2\ g^{-1}$ after being modified by HMDS. In this work, it is found that the surface charge property of the adsorbent is the key factor. The adsorption capacity of aerogels is in the order: Al_{HMD} > Al_{OSSD} > Si_{HMD} > Si_{OSSD}. The kinetic data are well fitted with the Lagergren first-order kinetics model according to the adsorption kinetics and the isotherm adsorption data are well fitted with the Langmuir model. The results of kinetic experiments and Langmuir isotherm confirm that, for all adsorbents, the adsorption proceeds *via* film diffusion and intra-particle diffusion. In short, the factors affecting dye adsorption are not only specific surface area and porosity, but also surface functional groups, electrostatic effect and surface charge. It is beneficial for designing a high-efficiency adsorbent to remove anionic aqueous contaminants.

Conflicts of interest

There are no conflicts to declare.

Acknowledgements

The authors gratefully acknowledge the financial support provided by the National Natural Science Foundation of China (21607063, 21676129), China Postdoctoral Science Foundation (2018M630530), and the Science & Technology Foundation of Zhenjiang (GY2017001).

References

1 E. Hu, X. Wu, S. Shang, X. M. Tao, S. X. Jiang and L. Gan, Catalytic ozonation of simulated textile dyeing wastewater using mesoporous carbon aerogel supported copper oxide catalyst, *J. Cleaner Prod.*, 2016, **112**, 4710–4718.

2 Z. F. Jiang, C. Z. Zhu, W. M. Wan, K. Qian and J. M. Xie, Constructing graphite-like carbon nitride modified hierarchical yolk–shell TiO_2 spheres for water pollution treatment and hydrogen production, *J. Mater. Chem. A*, 2016, **4**, 1806–1818.

3 C. Z. Liang, S. P. Sun, F. Y. Li, Y. K. Ong and T. S. Chung, Treatment of highly concentrated wastewater containing multiple synthetic dyes by a combined process of coagulation/flocculation and nanofiltration, *J. Membr. Sci.*, 2014, **469**, 306–315.

4 A. L. Ahmad, S. W. Puasa and S. Abiding, Crossflow ultrafiltration for removing direct-15 dye from wastewater of textile industry, *AJSTD*, 2017, **23**, 207–216.

5 M. M. Zheng, Y. J. Chi, H. W. Yi and S. L. Shao, Decolorization of Alizarin Red and other synthetic dyes by

a recombinant laccase from Pichia pastoris, *Biotechnol. Lett.*, 2014, **36**, 39–45.

6 R. Elmoubarki, F. Z. Mahjoubi, H. Tounsadi, J. Moustadraf, M. Abdennouri, A. Zouhri, A. El Albani and N. Barka, Adsorption of textile dyes on raw and decanted Moroccan clays: Kinetics, equilibrium and thermodynamics, *Water Resources and Industry*, 2015, **9**, 16–29.

7 S. H. Wu, H. J. He, X. Inthapanya, C. P. Yang, L. Lu, G. M. Zeng and Z. F. Han, Role of biochar on composting of organic wastes and remediation of contaminated soils-a review, *Environ. Sci. Pollut. Res.*, 2017, **24**(20), 16560–16577.

8 K. B. Tan, M. Vakili, B. A. Horri, P. E. Poh, A. Z. Abdullah and B. Salamatinia, Adsorption of dyes by nanomaterials: recent developments and adsorption mechanisms, *Sep. Purif. Technol.*, 2015, **150**, 229–242.

9 X. H. Duan, C. Srinivasakannan, X. Wang, F. Wang and X. Y. Liu, Synthesis of activated carbon fibers from cotton by microwave induced H_3PO_4 activation, *J. Taiwan Inst. Chem. Eng.*, 2017, **70**, 374–381.

10 H. C. Chen, W. Y. Cheng, Y. H. Wang and S. Y. Lu, Ultrahigh specific capacitances for supercapacitors achieved by nickel cobaltite/carbon aerogel composites, *Adv. Funct. Mater.*, 2012, **22**, 5038–5043.

11 W. T. Zhao, X. Q. Lu, M. Selvaraj, W. Wei, Z. F. Jiang, N. Ullah, J. Liu and J. M. Xie, M_XP(M = Co/Ni)@carbon core–shell nanoparticles embedded in 3D cross-linked graphene aerogel derived from seaweed biomass for hydrogen evolution reaction, *Nanoscale*, 2018, **10**, 9698–9706.

12 W. Li, F. Y. Li, F. L. Zhuo, M. J. Cao, Q. Cai, H. Jue, W. J. Zhang and M. W. Mu, Preparation of silica aerogels using CTAB/SDS as template and their efficient adsorption, *Appl. Surf. Sci.*, 2015, **353**, 1031–1036.

13 H. K. Han, W. Wei, Z. F. Jiang, J. W. Lu, J. J. Zhu and J. M. Xie, Removal of cationic dyes from aqueous solution by adsorption onto hydrophobic/hydrophilic silica aerogel, *Colloids Surf., A*, 2016, **509**, 539–549.

14 S. K. Zong, W. Wei, Z. F. Jiang, Z. X. Yan, J. J. Zhu and J. M. Xie, Characterization and comparison of uniform hydrophilic/hydrophobic transparent silica aerogel beads: skeleton strength and surface modification, *RSC Adv.*, 2015, **5**, 55579–55587.

15 Y. Q. Huang, C. P. Yang, Z. C. Sun, G. G. Zeng and H. J. He, Removal of cadmium and lead from aqueous solutions using nitrilotriacetic acid anhydride modified lignocellulosic material, *RSC Adv.*, 2015, **5**, 11475–11484.

16 C. P. Yang, J. Q. Wang, M. Lei, G. X. Xie, G. M. Zeng and S. L. Luo, Biosorption of zinc(II) from aqueous solution by dried activated sludge, *J. Environ. Sci.*, 2010, **22**(5), 675–680.

17 Y. Cheng, C. P. Yang, H. J. He, G. M. Zeng, K. Zhao and Z. Yan, Biosorption of Pb(II) ions from aqueous solution by waste biomass from biotrickling filters: kinetics, isotherms and thermodynamics, *J Environ Eng Ecol Sci.*, 2016, **142**(9), C40150.

18 W. Wei, P. Gao, J. M. Xie, S. K. Zong, H. L. Cui and X. J. Yue, Uniform $Cu_2Cl(OH)_3$ hierarchical microspheres: a novel adsorbent for methylene blue adsorptive removal from aqueous solution, *J. Solid State Chem.*, 2013, **204**, 305–313.

19 T. Matias, J. Marques, M. J. Quina, L. Gando-Ferreira, A. J. Valente, A. Portugal and L. Durães, Silica-based aerogels as adsorbents for phenol-derivative compounds, *Colloids Surf., A*, 2015, **480**, 260–269.

20 K. Shen and M. A. Gondal, Removal of hazardous Rhodamine dye from water by adsorption onto exhausted coffee ground, *J. Saudi Chem. Soc.*, 2017, **21**, S120–S127.

21 Y. F. Shi, B. K. Guo, S. A. Corr, Q. H. Shi, Y. S. Hu, K. R. Heier, L. Q. Chen, R. Seshadri and G. D. Stucky, Ordered mesoporous metallic MoO_2 materials with highly reversible lithium storage capacity, *Nano Lett.*, 2009, **9**, 4215–4220.

22 P. Pengthamkeerati, T. Satapanajaru and O. Singchan, Sorption of reactive dye from aqueous solution on biomass fly ash, *J. Hazard. Mater.*, 2008, **153**, 1149–1156.

23 W. B. Hu, M. M. Li, W. Chen, N. Zhang, B. Li, M. Wang and Z. M. Zhao, Preparation of hydrophobic silica aerogel with kaolin dried at ambient pressure, *Colloids Surf., A*, 2016, **501**, 83–91.

24 Y. F. Lei, X. H. Chen, H. H. Song, Z. J. Hu and B. Cao, Improvement of thermal insulation performance of silica aerogels by Al_2O_3 powders doping, *Ceram. Int.*, 2017, **43**, 10799–10804.

25 Y. C Chen, C. C. Tsai and Y. D. Lee, Preparation and properties of silylated PTFE/SiO_2 organic–inorganic hybrids *via* sol–gel process, *J. Polym. Sci., Polym. Chem.*, 2004, **42**, 1789–1807.

26 G. M. Walker and L. R. Weatherley, Adsorption of dyes from aqueous solution—the effect of adsorbent pore size distribution and dye aggregation, *Chem. Eng. J.*, 2001, **83**, 201–206.

27 J. Philipavičius, I. Kazadojev, A. Beganskienė and A. Kareiva, Hydrophobic antireflective silica coatings *via* sol-gel process, *Mater. Sci.*, 2008, **14**, 283–287.

28 A. C. Pierre, E. Elaloui and G. M. Pajonk, Comparison of the structure and porous texture of alumina gels synthesized by different methods, *Langmuir*, 1998, **14**, 66–73.

29 W. C. Li, A. H. Lu and S. C. Guo, Control of mesoporous structure of aerogels derived from cresol-formaldehyde, *J. Colloid Interface Sci.*, 2002, **254**, 153–157.

30 J. L. Mohanan and S. L. Brock, Influence of synthetic and processing parameters on the surface area, speciation, and particle formation in copper oxide/silica aerogel composites, *Chem. Mater.*, 2003, **15**, 2567–2576.

31 M. Thommes, K. Kaneko, A. V. Neimark, J. P. Olivier, F. Rodriguez-Reinoso, J. Rouquerol and K. S. Sing, Physisorption of gases, with special reference to the evaluation of surface area and pore size distribution (IUPAC Technical Report), *Pure Appl. Chem.*, 2015, **87**, 1051–1069.

32 S. D. Bhagat, Y. H. Kim, K. H. Suh, Y. S. Ahn, J. G. Yeo and J. H. Han, Superhydrophobic silica aerogel powders with simultaneous surface modification, solvent exchange and sodium ion removal from hydrogels, *Microporous Mesoporous Mater.*, 2008, **112**, 504–509.

33 Z. D. Shao, F. Z. Luo, X. Cheng and Y. Zhang, Superhydrophobic sodium silicate based silica aerogel prepared by ambient pressure drying, *Mater. Chem. Phys.*, 2013, **141**, 570–575.

34 V. K. Garg, R. Kumar and R. Gupta, Removal of malachite green dye from aqueous solution by adsorption using agro-industry waste: a case study of *Prosopis cineraria*, *Dyes Pigm.*, 2004, **62**, 1–10.

35 B. K. Nandi, A. Goswami and M. K. Purkait, Removal of cationic dyes from aqueous solutions by kaolin: kinetic and equilibrium studies, *Appl. Clay Sci.*, 2009, **42**, 583–590.

36 T. T. Ma, P. R. Chang, P. W. Zheng, F. Zhao and X. F. Ma, Fabrication of ultra-light graphene-based gels and their adsorption of methylene blue, *Chem. Eng. J.*, 2014, **240**, 595–600.

37 V. K. Gupta, A. Mittal, V. Gajbe and J. Mittal, Removal and recovery of the hazardous azo dye acid orange 7 through adsorption over waste materials: bottom ash and de-oiled soya, *Ind. Eng. Chem. Res.*, 2006, **45**, 1446–1453.

38 G. J. Millar, S. J. Couperthwaite, L. A. Dawes, S. Thompson and J. Spencer, Activated alumina for the removal of fluoride ions from high alkalinity groundwater: New insights from equilibrium and column studies with multicomponent solutions, *Sep. Purif. Technol.*, 2017, **187**, 14–24.

39 Y. Lin, S. H. Wu, X. Li, X. Wu, C. P. Yang, G. M. Zeng, Y. R. Peng, Q. Zhou and L. Lu, Microstructure and performance of Z-scheme photocatalyst of silver phosphate modified by MWCNTs and Cr-doped $SrTiO_3$ for malachite green degradation, *Appl. Catal., B*, 2018, **227**, 557–570.

40 C. Zhang, S. G. Yang, H. Z. Chen, H. He and C. Sun, Adsorption behavior and mechanism of reactive brilliant red X-3B in aqueous solution over three kinds of hydrotalcite-like LDHs, *Appl. Surf. Sci.*, 2014, **301**, 329–337.

41 M. T. Roy, M. Gallardo and J. Estelrich, Influence of size on electrokinetic behavior of phosphatidylserine and phosphatidylethanolamine lipid vesicles, *Colloid Interface Sci.*, 1998, **206**, 512–517.

42 O. E. Gholabzouri, M. A. Cabrerizo and R. H. Alvarez, The surface charge density influence on the electrokinetic properties of model colloids; solvent composition effect, *Colloid Interface Sci.*, 1999, **214**, 243–250.

43 F. McNeil-Watson, W. Tscharnuter and J. Miller, A new instrument for the measurement of very small electrophoretic mobilities using phase analysis light scattering, *Colloids Surf.*, 1998, **140**, 53–57.

44 K. C. Leonard, J. R. Genthe, J. L. Sanfilippo, W. A. Zeltner and M. A. Anderson, Synthesis and characterization of asymmetric electrochemical capacitive deionization materials using nanoporous silicon dioxide and magnesium doped aluminum oxide, *Electrochim. Acta*, 2009, **54**, 5286–5291.

45 P. S. Suchithra, L. Vazhayal, A. P. Mohamed and S. Ananthakumar, Mesoporous organic–inorganic hybrid aerogels through ultrasonic assisted sol–gel intercalation of silica–PEG in bentonite for effective removal of dyes, volatile organic pollutants and petroleum products from aqueous solution, *Chem. Eng. J.*, 2012, **200**, 589–600.

46 M. K. Dwivedi, R. Agrawal and P. Sharma, Adsorptive Removal of Methylene Blue from Wastewater Using Zeolite-Iron Oxide Magnetic Nanocomposite, *IJARSE*, 2016, **5**, 515–522.

47 M. T. Yagub, T. K. Sen and H. M. Ang, Equilibrium, kinetics and thermodynamics of methylene blue adsorption by pine tree leaves, *Water, Air, Soil Pollut.*, 2012, **223**, 5267–5282.

48 A. H. Sulaymon, W. M. Abood, T. J. Al-Musawi and D. Ali, Single and binary adsorption of reactive blue and red dyes onto activated carbon, *IJEIR*, 2014, **3**, 642–649.

49 S. Dawood and T. K. Sen, Removal of anionic dye Congo red from aqueous solution by raw pine and acid-treated pine cone powder as adsorbent: equilibrium, thermodynamic, kinetics, mechanism and process design, *Water Res.*, 2012, **46**, 1933–1946.

50 T. G. Venkatesha, R. Viswanatha, Y. A. Nayaka and B. K. Chethana, Kinetics and thermodynamics of reactive and vat dyes adsorption on MgO nanoparticles, *Chem. Eng. J.*, 2012, **198**, 1–10.

51 L. Lin, Z. F. Lei, L. Wang, X. Liu, Y. Zhang, C. L. Wan, D. J. Lee and J. H. Tay, Adsorption mechanisms of high-levels of ammonium onto natural and NaCl-modified zeolites, *Sep. Purif. Technol.*, 2013, **103**, 15–20.

52 Z. C. Li, G.-Q. Wang, K. L. Zhai, C. C. He, Q. Li and P. Z. Guo, Methylene blue adsorption from aqueous solution by loofah sponge-based porous carbons, *Colloids Surf., A*, 2018, **538**, 28–35.

53 S. J. Allen, G. Mckay and K. Y. H. Khader, Intraparticle diffusion of a basic dye during adsorption onto sphagnum peat, *Environ. Pollut.*, 1989, **56**, 39–50.

54 T. K. Sen, S. Afroze and H. M. Ang, Equilibrium, kinetics and mechanism of removal of methylene blue from aqueous solution by adsorption onto pine cone biomass of Pinus radiate, *Water, Air, Soil Pollut.*, 2011, **218**, 499–515.